ADVANCES IN ATMOSPHERIC SCIENCES, VOL. 39, JULY 2022, 1062–1078

• **Original Paper** •

Comparative Analysis of the Characteristics of Rainy Season Raindrop Size Distributions in Two Typical Regions of the Tibetan Plateau※

Gaili WANG*, Ran LI, Jisong SUN, Xiangde XU, Renran ZHOU, and Liping LIU

State Key Laboratory of Severe Weather, *Chinese Academy of Meteorological Science*, *Beijing* 100081, *China*

(Received 8 April 2021; revised 7 September 2021; accepted 9 October 2021)

ABSTRACT

Mêdog and Nagqu are two typical regions of the Tibetan Plateau with different geographical locations and climate regimes. These differences may lead to discrepancies in the raindrop size distributions (DSDs) and precipitation microphysical processes between the two regions. This paper investigates discrepancies in the DSDs using disdrometer data obtained during the rainy season in Mêdog and Nagqu. The DSD characteristics are studied under five different rainfall rate categories and two precipitation types (stratiform and convective). For the total datasets, the number concentrations of drops with diameters $D > 0.6$ ($D < 0.6$) mm are higher (lower) in Nagqu than in Mêdog. The fitted normalized gamma distributions of the averaged DSDs for the five rainfall rate categories show that Nagqu has a larger (lower) mass-weighted mean diameter D_m (normalized intercept parameter, $\lg N_w$) than Mêdog does. The difference in D_m between Nagqu and Mêdog increases with the rainfall rate. Convective clusters in Nagqu could be identified as continental-like, while convective precipitation in Mêdog could be classified as maritime-like. The relationships between the shape factor μ and slope parameter Λ of the gamma distribution model, the radar reflectivity Z, and the rainfall rate R are also derived. Furthermore, the possible causative mechanism for the notable DSD variation between the two regions during the rainy season is illustrated using reanalysis data and automated weather station observations. Cold rain processes are mainly responsible for the lower concentrations of larger drops observed in Nagqu, whereas warm rain prevails in Mêdog, producing abundant small drops.

Key words: raindrop size distribution, Tibetan Plateau, continental-like, maritime-like, warm rain, cold rain

Citation: Wang, G. L., R. Li, J. S. Sun, X. D. Xu, R. R. Zhou, and L. P. Liu, 2022: Comparative analysis of the characteristics of rainy season raindrop size distributions in two typical regions of the Tibetan Plateau. *Adv. Atmos. Sci.*, **39**(7), 1062−1078, https://doi.org/10.1007/s00376-021-1135-6.

Article Highlights:

- Convective clusters in Nagqu could be identified as continental-like, while convective rain in Mêdog could be classified as maritime-like.
- Cold rain contributes to the low concentrations of large drops in Nagqu, while warm rain prevails in Mêdog, producing abundant small drops.

1. Introduction

The Tibetan Plateau (TP) has the most abundant water resources (such as glaciers, rivers, and lakes) and the highest altitude in the world. The TP not only plays a significant role in the formation of Asian monsoon circulations but also has a profound impact on the global water cycles, climate, and environment (Xu et al., 2014, 2015; Wan et al., 2017). Clouds and precipitation over the TP are important components of global hydrological cycles and energy budgets (Xu et al., 2008; Kang et al., 2010; Li, 2018). However, the shortage of in situ observations and the low spatiotemporal resolution and uncertainties in satellite measurements have restricted the understanding of the physical properties of clouds and precipitation over the TP (Zhao et al., 2019).

To strengthen the observations of clouds and precipitation over the TP, three Tibetan Plateau Atmospheric Scientific Experiments (TIPEX) were carried out in the summers of 1979, 1998, and 2013 (Liu et al., 2002; Chen et al., 2017; Zhao et al., 2018, 2019). In particular, during the third TIPEX, advanced measurements such as Ka-band cloud radar, X-band dual polarization radar, disdrometers, and microwave radiometers were deployed in Nagqu on the TP to comprehensively analyze the physical properties and

※ This paper is a contribution to the special issue on Third Pole Atmospheric Physics, Chemistry, and Hydrology.

* Corresponding author: Gaili WANG
Email: wanggl@cma.gov.cn

climatic characteristics of clouds and precipitation (Liu et al., 2015; Chang and Guo, 2016; Chen et al., 2017).

However, due to the complex topography of the TP, the representativeness of single station observations is very poor. Therefore, the Second Tibetan Plateau Scientific Expedition and Research (STEP) project and the "Earth-Atmosphere Interaction in the TP and its Influence on the Weather and Climate in the Lower Reaches" project were launched to establish several field observation campaign sites at which to examine clouds and precipitation in 2019. In particular, Mêdog, located in front of the main water vapor channel over the TP, is a very important campaign site where an X-band polarization phased array radar, a Ka-band cloud radar, a microwave radiometer, a disdrometer, and other instruments were deployed intermittently by the Chinese Academy of Meteorological Sciences (CAMS). One of the precise scientific objectives at this site is to obtain the development and precipitation characteristics of convective clouds in the valley of the Yarlung Zangbo Grand Canyon (YZGC).

The raindrop size distribution (DSD) has received much attention over the past few decades due to its great importance in reflecting the fundamental microphysics of rainfall (Rosenfeld and Ulbrich, 2003). A better understanding of the DSD and its variation is not only critical for microphysical parameterizations in numerical weather prediction models (Milbrandt and Yau, 2005; Morrison and Milbrandt, 2015) but is also important for the remote sensing of precipitation (Cifelli et al., 2011; Chen et al., 2017). Microphysical parameterization is a key element in numerical models that affects the prediction accuracy of convective systems (Gilmore et al., 2004; Krishna et al., 2016). Quantitative precipitation estimations (QPEs) from ground-based weather radar or spaceborne satellite observations depend on the characteristics of the DSD to develop rainfall retrieval algorithms (Zhang et al., 2001; Chandrasekar et al., 2005; Lam et al., 2015; Ji et al., 2019). To this end, numerous DSD observations have been conducted around the world to elucidate the variability in DSDs among different climate regions and rainfall types (Tokay and Short, 1996; Yuter and Houze, 1997; Maki et al., 2001; Testud et al., 2001; Bringi et al., 2003; Zhang et al., 2003; Thurai, et al., 2010; Lam et al., 2015; Chen et al., 2016, 2017; Wu et al., 2019; Ji et al., 2019).

In the last several decades, many DSD studies have also been conducted over various regions in China using optical disdrometers. Most of these studies were carried out in eastern and southern China (Niu et al., 2010; Chen et al., 2013, 2016; Tang et al., 2014; Wang et al., 2015; Wen et al., 2016; Wu and Liu, 2017; Huo et al., 2019). Recently, the DSD characteristics over the TP were studied using disdrometer data collected at Lhasa [3600 m above sea level (ASL)] and Nyingchi (3300 m ASL), and it was revealed that collisional breakup occurred at a lower rainfall intensity and with a smaller maximum raindrop size than that in low-altitude regions (Porcù et al., 2014). Based on DSD measurements taken at Nagqu (31.29°N, 92.04°E; 4508 m ASL) during the third TIPEX, Chen et al. (2017) showed that convective precipitation was characterized by smaller generalized intercepts (N_w) and larger mass-weighted mean diameters (D_m) in the daytime than at nighttime. However, complex topography and underlying surface characteristics over the TP limit the representativeness of observations from any specific station.

In June 2019, a particle size and velocity (PARSIVEL) disdrometer was deployed at the Mêdog National Climate Observatory (MNCO; 29.31°N, 95.32°E; 1275 m ASL) to perform continuous raindrop spectra measurements. Mêdog and Nagqu are two typical regions of the TP with different geographical locations and climate regimes (Fig. 1). Mêdog is located on the southern slope of the Himalayas at the entrance of the water vapor transport channel of the YZGC, which is the most important water vapor channel through which the Indian Ocean monsoon affects precipitation over the TP (Yang et al., 1987; Zhang et al., 2016). Mêdog has a mean altitude of 1200 m ASL and subtropical climatic characteristics. The warm and wet water vapor from the Indian Ocean leads to a large amount of total precipitation in Mêdog with an annual average rainfall of more than 2000 mm (Chen and Li, 2018). Precipitation is mainly concentrated from June to September, accounting for 64% of the total annual precipitation. Nagqu is located in the center of the TP, with a mean altitude exceeding 4500 m ASL and a plateau mountain climate. Its mean annual precipitation is approximately 400 mm, and over 80% of the total precipitation occurs in summer (Chen et al., 2017). In summer, the Indian Ocean monsoon brings abundant water vapor to Mêdog, while the Nagqu region experiences interactions between the westerly wind and Indian Ocean monsoon (Yang et al., 1987; Zhang et al., 2016; Zeng et al., 2020).

Therefore, the objectives of this study are to (i) explore if there were any distinct discrepancies of DSD characteristics and precipitation microphysical processes between Mêdog and Nagqu, considering the different sources of water vapor and topography in the two regions; (ii) investigate the possible causative meteorological factors if a notable DSD discrepancy does exist between the two regions of the TP; and (iii) better understand the DSD characteristics in Mêdog and Nagqu over the TP, providing a basis for improving the microphysical parameterization scheme of the numerical model over the TP. These objectives will be achieved through a comparative study on the DSD variations in precipitation between Mêdog and Nagqu based on DSD measurements taken in Mêdog during the STEP field campaign and in Nagqu during the third TIPEX. In addition to the PARSIVEL disdrometer, the automated weather station (AWS) data of the China Meteorological Administration, Moderate Resolution Imaging Spectroradiometer (MODIS) data products, and the European Centre for Medium-Range Weather Forecasts (ECMWF) Reanalysis version 5 (ERA5) are combined to illustrate the microphysical characteristics of precipitation in two regions of the TP.

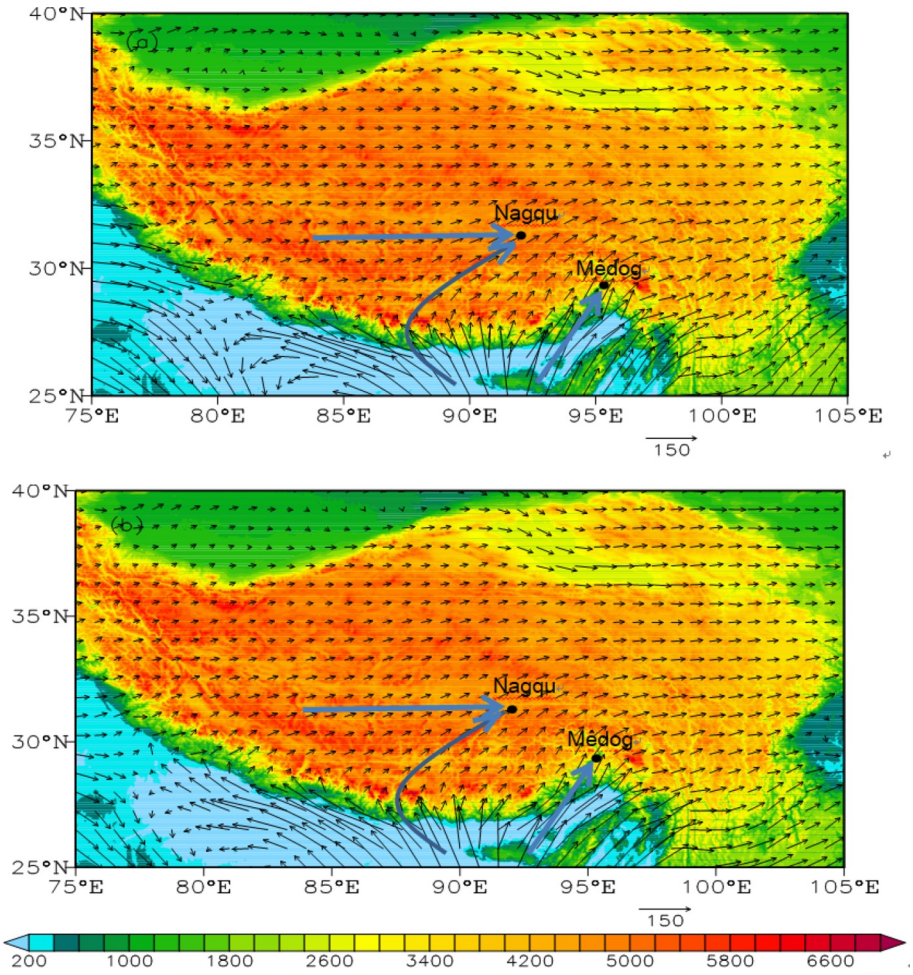

Fig. 1. Locations of the Mêdog and Nagqu observation fields (black dots), the topography (m, shaded) of the Tibetan Plateau (TP) superimposed with the mean vertical integral of the water vapor flux obtained in summer of (a) 2014 and (b) 2019 (kg m^{-1} s^{-1}, thin black arrows), and the trajectories of the water vapor (thick gray arrows).

The instruments and methodology adopted in this study are described in section 2. The observational results in terms of the DSD characteristics of different rainfall rates and precipitation types in Mêdog and Nagqu are presented in section 3. The possible reasons for the observed variations in the DSDs of the two regions of the TP are discussed in section 4. A summary and conclusion are given in the final section.

2. Instruments and methods

High-resolution (1-min) DSD data collected with PARSIVEL disdrometers are used in the present study. The DSD data of Mêdog were measured from June to September 2019 during the STEP field campaign, and the DSD data of Nagqu were collected from June to August 2014 and from July to August 2015 during the third TIPEX due to no observations in Nagqu in 2019 during STEP. Based on the analysis of the average vertical cumulative water vapor fluxes of Nagqu and Mêdog from June to August in 2014–19, the water vapor sources of Nagqu and Mêdog are basically unchanged (mean vertical cumulative water vapor fluxes in summer seasons of 2014 and 2019 are given in Fig. 1). In summer, Nagqu is affected jointly by the westerly wind and Indian Ocean monsoon, while Mêdog is dominated by the Indian Ocean monsoon. Therefore, the data of different years will not impact the main DSD characteristics of Nagqu and Mêdog.

The PARSIVEL disdrometer is one of the most common instruments used around the globe to understand the microphysical processes of rainfall for several decades (Yuter et al., 2006; Niu et al., 2010; Chen et al., 2013, 2017; Friedrich et al., 2013; Tokay et al., 2013; Wen et al, 2016; Wu and Liu, 2017; Ji et al., 2019; Wu et al., 2019). This disdrometer is capable of the simultaneous measurements of the diameter and fall speed of hydrometeors near the ground. The measured hydrometeors are separated into 32 nonequidistant size categories with a range of 0.062–24.5 mm and 32 nonequidistant terminal velocity categories with a range of 0.05–20.8 m s^{-1} (Chen et al., 2017; Wu and Liu, 2017). The bin widths of the diameter (terminal velocity) categories increase from 0.125 mm (0.1 m s^{-1}) to 3.0 mm

(3.2 m s^{-1}) with increasing particle size. The sampling area of the PARSIVEL disdrometer is 54 cm^2.

In addition to the PARSIVEL disdrometer, MODIS, AWS, and ECMWF ERA5 data were also collected. Rainfall data measured from a tipping-bucket gauge with a 0.1-mm resolution and a 1-min interval were used as the ground truth. The daily averages of surface meteorological variables (such as temperature, relative humidity, and horizontal winds) measured by AWSs were considered for rainy days over the two typical regions of the TP. The ECMWF ERA5 reanalysis data were obtained on regular latitude–longitude grids at a spatial resolution of 0.25° × 0.25°. Hourly ERA5 reanalysis data of rainy days with 37 pressure levels in the vertical direction were used to obtain the mean temperature and relative humidity profiles in Mêdog and Nagqu, and monthly mean ERA5 reanalysis data with single level were used to obtain the distribution of the vertical integral of water vapor flux over the TP. Cloud top height (CTH) products from MODIS were also used.

From the disdrometer counts, the raindrop concentration, $N(D_i)$ (mm^{-1} m^{-3}), in diameter category i can be expressed as follows:

$$N(D_i) = \sum_{j=1}^{32} \frac{n_{i,j}}{V_j A \Delta t \Delta D_i}, \tag{1}$$

where $n_{i,j}$ represents the number of drops within the diameter category i and the velocity category j; D_i (mm) indicates the average drop diameter for diameter category i; ΔD_i (mm) is the corresponding diameter interval; V_j (m s^{-1}) represents the terminal velocity for speed category j; and A (m^2) and Δt (s) are the sampling area (54 cm^2 in the present study) and time interval (60 s in the present study), respectively. The radar reflectivity factor Z (mm^6 m^{-3}), rainwater content W (g m^{-3}), rainfall rate R (mm h^{-1}), and total raindrop concentration N_t (m^{-3}) can be obtained from the equations below.

$$Z = \sum_{i=1}^{32} N(D_i) {D_i}^6 \Delta D_i, \tag{2}$$

$$W = \frac{\pi}{6} \times 10^{-3} \sum_{i=1}^{32} N(D_i) {D_i}^3 \Delta D_i, \tag{3}$$

$$R = 6\pi \times 10^{-4} \sum_{i=1}^{32} \sum_{j=1}^{32} N(D_i) {D_i}^3 V_j \Delta D_i, \tag{4}$$

$$N_t = \sum_{i=1}^{32} N(D_i) \Delta D_i. \tag{5}$$

The observed DSDs are fitted with the three-parameter gamma distribution model, expressed in the following form (Ulbrich, 1983):

$$N(D) = N_0 D^{\mu} \exp(-\Lambda D), \tag{6}$$

where D (mm) indicates the hydrometeor size and $N(D)$ (m^{-3} mm^{-1}) represents the numbers of hydrometeors within each unit volume and unit size interval. The three-parameter gamma distribution is widely expressed with the intercept parameter N_0 (m^{-3} $mm^{-1-\mu}$), shape factor μ, and slope parameter Λ (mm^{-1}). The method of moments (MoM) was used to estimate these integral rainfall parameters in our study because of its easy implementation and ability to proportionally fit the moments of the parameters.

The nth-order moment of the DSD, M_n, is described as follows.

$$M_n = \sum_{i=1}^{32} N(D_i) {D_i}^n \Delta D_i. \tag{7}$$

The three-parameter gamma distribution can be calculated as follows (Kozu and Nakamura, 1991):

$$\mu = \frac{11G - 8 + \sqrt{G(G+8)}}{2(1-G)}, \tag{8}$$

where:

$$G = \frac{M_4^3}{M_3^2 M_6}, \tag{9}$$

$$\Lambda = (\mu + 4)\frac{M_3}{M_4}, \tag{10}$$

$$N_0 = \frac{\Lambda^{\mu+4} M_3}{\Gamma(\mu+4)}, \tag{11}$$

where $\Gamma(x)$ represents a complete gamma function that is defined as follows.

$$\Gamma(x) = \sqrt{2\pi} e^{-x} x^{x-\frac{1}{2}}. \tag{12}$$

The normalized intercept parameter N_w (m^{-3} mm^{-1}) and the mass-weighted mean diameter D_m (mm) were defined by Smith (2003) as follows.

$$N_w = \frac{256 M_3^5}{6 M_4^4}, \tag{13}$$

$$D_m = \frac{M_4}{M_3}. \tag{14}$$

The advantages and disadvantages of the PARSIVEL disdrometer are well understood from previous studies (Yuter et al., 2006; Jaffrain and Berne, 2011; Friedrich et al., 2013; Tokay et al., 2013; Wen et al., 2017). The PARSIVEL disdrometer is unable to resolve the effects of margin fallers, winds, and splashing (Yuter et al., 2006; Friedrich et al., 2013). Therefore, fallers outside the range of ±60% of the

empirical terminal velocity–diameter relationship determined by Atlas et al. (1973) were removed. Before filtering spurious drops, the air density correction factors of 1.04 and 1.20 were multiplied by the terminal velocity–diameter relationship considering the terrain heights of Mêdog and Nagqu on the TP, respectively (Atlas et al., 1973). The first two diameter categories with low signal-to-noise ratios and the last ten diameter categories with drop size greater than 8 mm were left empty (Wu and Liu, 2017). Thus, the DSD is calculated for drop diameters from 0.31 to 8.0 mm. In addition, 1-min DSD samples collected by the disdrometers should be abandoned if the total drop counts are less than 10 (Tokay et al., 2013). As shown in Fig. 2, the distribution of raindrop terminal velocities and diameters conformed to the empirical relationship after quality control. Figure 2 also shows that the number concentration of large drops ($D \geqslant 3$ mm) was significantly higher in Nagqu than in Mêdog. Finally, there were 47 774 1-min effective DSD data points for Mêdog and 18 578 for Nagqu. For the quality validation of the PARSIVEL disdrometer data, Fig. 3 gives two examples (one for Mêdog and the other for Nagqu) comparing the time series of the 5-min mean rainfall rates derived from disdrometer with those from the tipping bucket rain gauges. Scatterplots of the hourly rainfall data used in this study, measured by disdrometer and rain gauge, are also given in Fig. 3. In general, reasonably good consistencies between the two measurement means are evident. For example, the DSD data reflected the rapid changes in precipitation intensity in both Mêdog and Nagqu, although the rainfall rate was slightly underestimated (e.g., Figs. 3b and e); the correlation coefficients (CC) of hourly rainfall between disdrometer and rain gauge are higher than 0.85, and the biases are less than 20.0% (Figs. 3c and f). These biases are in line with the instrument uncertainties of approximately 15%–20% biases for various rainfall events compared to rain gauge data (Krajewski et al., 2006; Tokay et al., 2013; Wen et al., 2017). It is noted that the bias in Mêdog is greater than that in Nagqu. Wen et al. (2017) reported that the PARSIVEL disdrometer tends to underestimate the number of small ($D < 1$ mm) and midsize ($1 < D < 3$ mm) raindrops because of the "one drop at once" assumption and the method used to measure laser signals. The known underestimation of small and medium raindrops, which are prevalent in Mêdog precipitation, may be the main reason for the greater bias observed in Mêdog than in Nagqu.

3. Results

3.1. *DSD variation of different precipitation intensity*

To examine the precipitation characteristics in the two regions of the TP, the DSD observations from Mêdog and Nagqu were divided into five categories on the basis of rainfall rate (R): $R \leqslant 0.1$ mm h^{-1}, $0.1 < R \leqslant 1$ mm h^{-1}, $1 < R \leqslant 5$ mm h^{-1}, $5 < R \leqslant 10$ mm h^{-1}, and $R > 10$ mm h^{-1}. The accumulated rain amounts (averaged rain rates) of the five categories in Mêdog are 9.04 mm (0.034 mm h^{-1}), 143.12 mm (0.42 mm h^{-1}), 346.14 mm (1.98 mm h^{-1}), 74.42 mm (6.73 mm h^{-1}), and 63.43 mm (17.62 mm h^{-1}), respectively. Nagqu has accumulated rain amounts (averaged rain rates) of 2.90 mm (0.043 mm h^{-1}), 52.20 mm (0.42 mm h^{-1}), 234.13 mm (2.31 mm h^{-1}), 93.16 mm (6.75 mm h^{-1}), and 155.57 mm (22.66 mm h^{-1}), respectively. Figure 4 gives the relative contributions of the five rainfall rate categories to the cumulative rainfall durations and rainfall totals in Mêdog and Nagqu. In Mêdog, weak precipitation with $R < 1$ mm h^{-1} often occurred, contributing more than 70% of the rainfall occurrences recorded during the observation periods in this study. In Nagqu, the second and third rainfall rate categories ($0.1 < R \leqslant 5$ mm h^{-1}) were the two largest contributors and were responsible for 72% of the cumulative rainfall durations. The largest contributor to the total rainfall

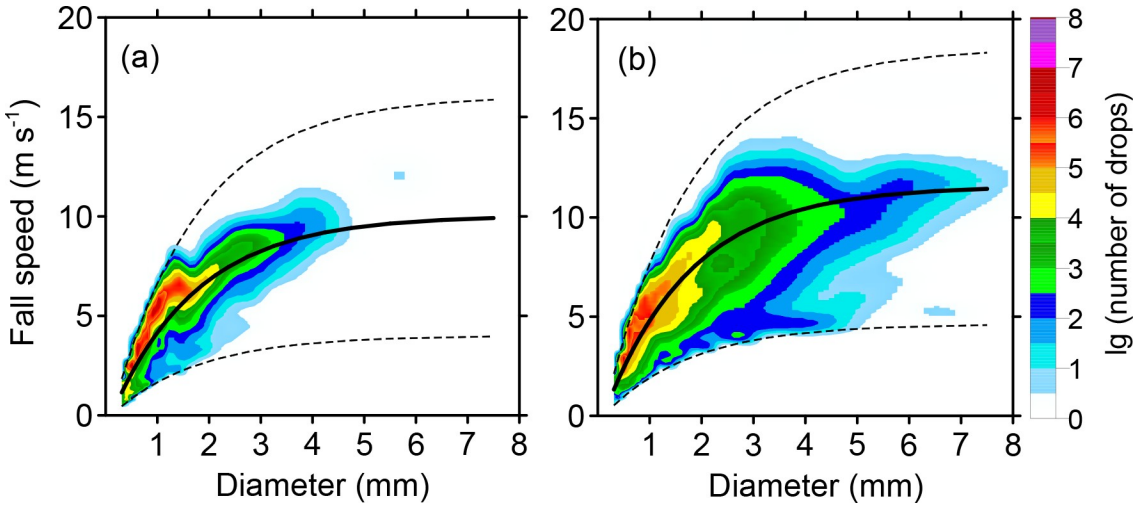

Fig. 2. Cumulative, corrected numbers of drops by diameter and terminal velocity in the total observation data of (a) Mêdog and (b) Nagqu used in this study. The solid black lines represent the empirical fall velocity–diameter relation reported by Atlas et al. (1973), which was multiplied by the air-density correction factors of 1.04 and 1.20 in Motu and Nagqu, respectively. The dashed black lines denote the ±60% empirical fall velocity–diameter relation.

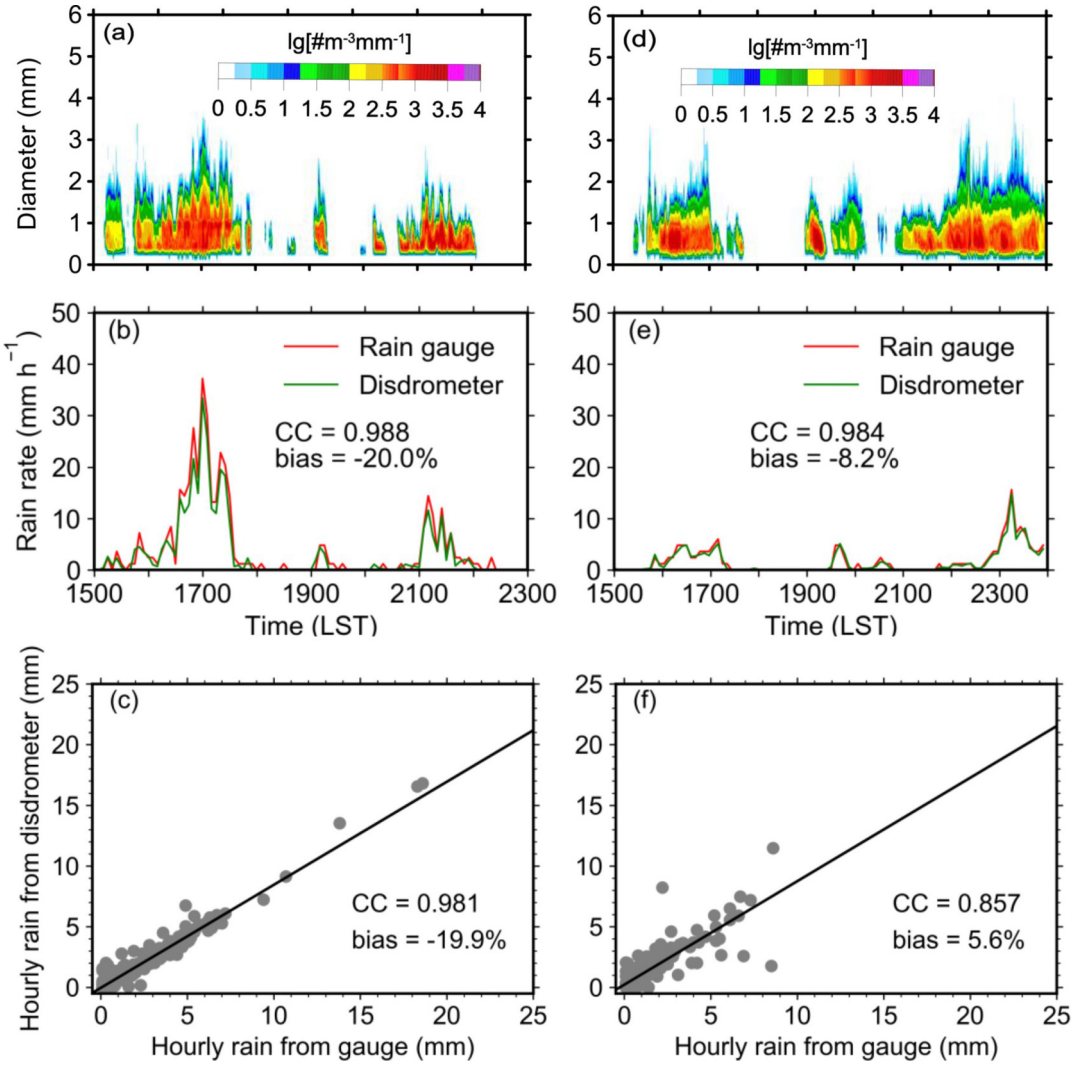

Fig. 3. Time-series drop size distribution (DSD) (a) from 1500 to 2300 LST 12 September 2019 in Mêdog and (c) from 1500 LST 16 July to 0000 LST 17 July 2014 in Nagqu; comparison of 5-min mean rain rates (mm h^{-1}) derived from the PARSIVEL disdrometer (green lines) and those obtained from rain gauges (red lines) in (b) Mêdog and (d) Nagqu; comparison of hourly rainfall between disdrometer and rain gauge in Mêdog (c) and Nagqu (f).

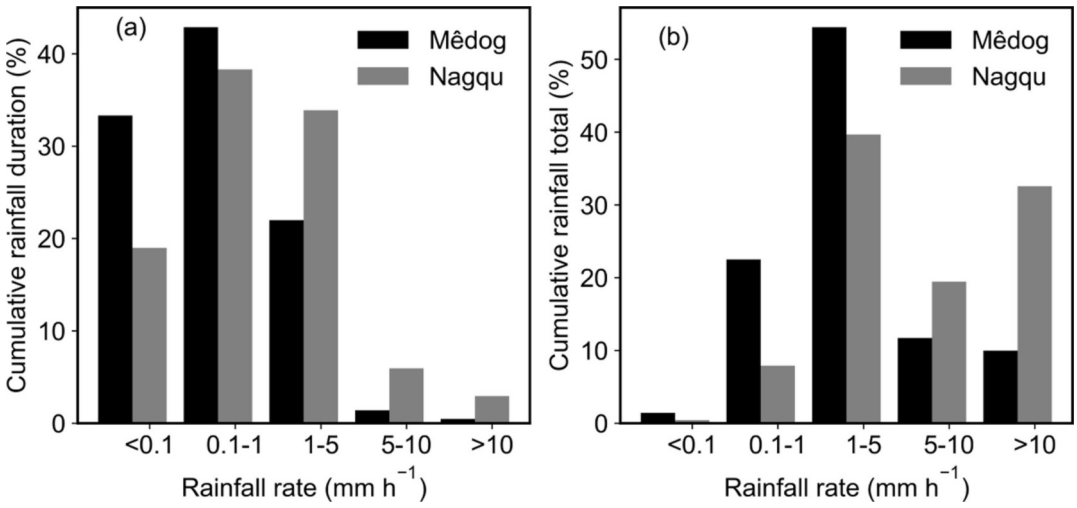

Fig. 4. Relative contributions of each rainfall rate category to the (a) cumulative rainfall durations (min) and (b) cumulative rainfall totals (mm) in Mêdog and Nagqu on the TP.

amount was the third category ($1 < R \leqslant 5$ mm h^{-1}) in both regions; this category was responsible for 54% and 40% of the cumulative rainfall totals in Mêdog and Nagqu, respectively.

The mean DSDs of the five rainfall rate categories and the total datasets in Mêdog and Nagqu are depicted in Fig. 5. In general, in the DSDs of the two regions of the TP, both the spectral widths and the large-drop concentrations increase with rainfall rate. It is also evident from the figure that the number concentrations of small drops are higher in Mêdog than in Nagqu for all rainfall rate categories. However, the number concentration of large drops is higher in Nagqu than in Mêdog. This discrepancy in the number concentration of large drops between Nagqu and Mêdog increases with increased rainfall rates. Distinct differences in the DSDs between Mêdog and Nagqu are noticeable in the rainfall rate categories above 5 mm h^{-1}. In Mêdog, lower rainfall rate categories ($\leqslant 5$ mm h^{-1}) show one peak distribution, and higher rainfall rate categories (> 5 mm h^{-1}) show two peak distributions (e.g., peaks at 0.5 mm and 1.1 mm). However, all rainfall rate categories in Nagqu show one apparent peak distribution. The multipeak character of DSD has been studied based on different disdrometer measurements at different locations in Switzerland from 1982 to 1986 (Steiner and Waldvogel, 1987). Multiple peaks of DSD were also observed by ground-based Doppler radar in Denver (Gossard et al., 1990). Srivastava (1971) pointed out that size distribution of raindrops may not have established equilibrium in the observed falling distance. Therefore, convective rainfall with a melting level at a higher altitude increases the probability for the multipeak behavior because of the long fall distances of raindrops (List et al., 1987).

The average raindrop concentrations with drop diameters in the total datasets collected in Mêdog and Nagqu are depicted in Fig. 5f. It is apparent that the number concentrations of midsize and large drops are higher in Nagqu than in Mêdog, whereas the number concentration of drops with diameters smaller than 0.6 mm is lower in Nagqu than in Mêdog.

The largest uncertainty in model predictions of convective precipitation originates from microphysical parameterizations (Krishna et al., 2016). Therefore, one of the most important aspects of DSD research is to improve the parameterization scheme of the cloud–precipitation microphysical processes in numerical models. For this purpose, the Mêdog and Nagqu precipitation DSDs observed from disdrometers are fitted to gamma distributions (Eq. 6) by using MOM. The D_m, N_w, μ, and Λ variations based on the rainfall rate categories in Mêdog and Nagqu are given in Fig. 6.

The average D_m values have similar trends at the two sites, continuously increasing with the rainfall rate in both regions. This feature is in line with the results of previous studies and is a result of the enhancement of large raindrops with increasing rainfall rate (Testud et al., 2001; Rosenfeld and Ulbrich, 2003). Nagqu has higher (lower) average D_m ($\lg N_w$) values than those of Mêdog for all rainfall rate categories. The discrepancy in the average D_m values between Nagqu and Mêdog increases with rainfall rate and changes from 0.115 mm to 0.568 mm.

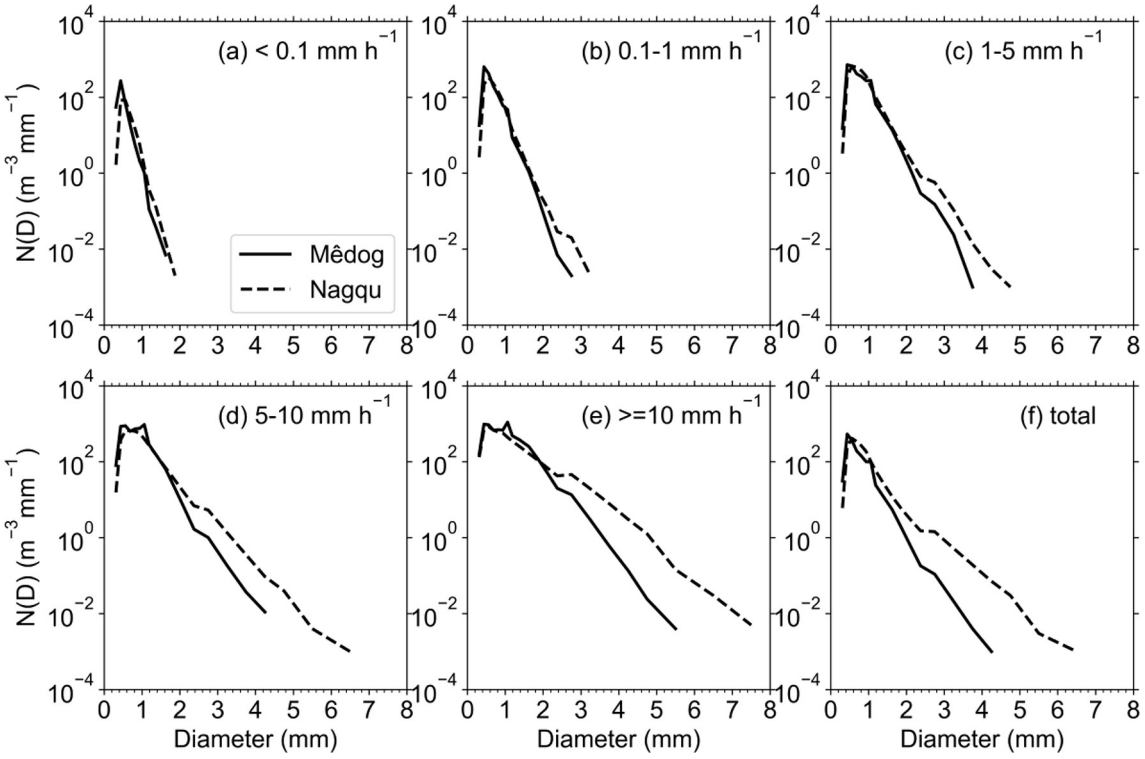

Fig. 5. Comparison of the mean DSDs obtained for different rainfall rate categories in Mêdog (solid lines) to those obtained for Nagqu (dashed lines) on the TP.

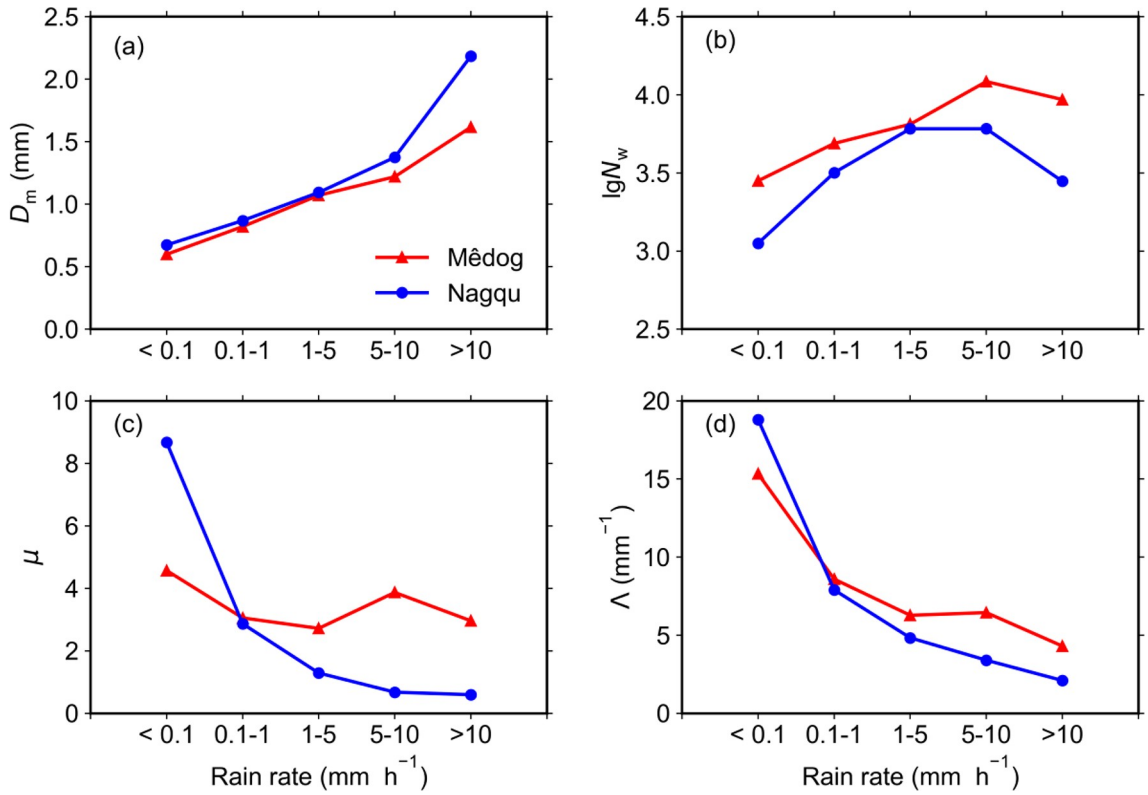

Fig. 6. Variations in the average D_m, lgN_w, μ and Λ values for each rainfall rate category in Mêdog and Nagqu.

The average lgN_w values increase up to rainfall rate category four (below 10 mm h^{-1}) and then decrease in both regions. In particular, the differences in both D_m and lgN_w between Nagqu and Mêdog were significant when the rainfall rate was higher than 10 mm h^{-1}. A rainfall rate higher than 10 mm h^{-1} is usually determined by convective clouds (Tokay and Short, 1996; Wu et al., 2019). That is, for convective precipitation with the same rainfall rate (corresponding to the same rainwater content), smaller drops with larger number concentrations were dominant in Mêdog, whereas Nagqu had a higher number concentration of large drops than Mêdog.

The average μ values are higher in Mêdog than in Nagqu, except for those of the first rainfall rate category ($R \leqslant 0.1$ mm h^{-1}). The average μ values in Nagqu show a monotonic decrease with an increasing rainfall rate and range from 8.676 to 0.598. The μ values in Mêdog decrease from 4.572 to 2.720 with an increasing rainfall rate, increase to 3.869 at R ranging from 5 to 10 mm h^{-1}, and then decrease again to 2.963 when $R > 10$ mm h^{-1}. The variation trends in the Λ values are found to be similar to those in the μ values, which may be due to the μ-Λ relation of $\Lambda D_m = 4 + \mu$. The Λ values range from 4.308–15.328 mm^{-1} (2.105–18.803 mm^{-1}) in Mêdog (Nagqu).

3.2. *DSDs in different precipitation types*

Studies have shown that the microphysical dynamics of raindrop spectra are significantly different in different precipitation types (Tokay and Short, 1996; Bringi et al., 2003; Ulbrich and Atlas, 2007). Therefore, we investigated the DSD characteristics of stratiform and convective precipitation types in Mêdog and Nagqu. Due to the scarcity of observation instruments on the TP, a simple stratification method proposed by Bringi et al. (2003) based on the standard deviation (STD) of the rainfall rate over ten consecutive 1-min DSD samples was used in this study. If the STD $\leqslant$ 1.5 mm h^{-1}, stratiform precipitation is identified; if the STD > 1.5 mm h^{-1} and $R > 5$ mm h^{-1}, convective precipitation is identified. As a result, the data from Mêdog and Nagqu consist of 95.1%/1.5% (45 426/707) and 88.2%/5.4% (16 393/995) stratiform/convective rain samples, respectively. For stratiform precipitation in Mêdog/Nagqu, the accumulated rain amount and mean rain rate were 448 mm/266 mm and 0.6 mm h^{-1}/1.0 mm h^{-1}, respectively. For convective precipitation, the accumulated rain amount and mean rain rate were 110 mm/222 mm and 9.3 mm/13.4 mm h^{-1}, respectively.

The relative-frequency histograms of D_m and lgN_w values derived from 1-min DSD samples for stratiform and convective precipitation events in Mêdog and Nagqu are given in Fig. 7. Regarding the stratiform precipitation type (Figs. 7a and c), the patterns of the D_m and lgN_w distributions in Mêdog are generally close to those in Nagqu, as are the statistical values [mean value (MEAN), standard deviation (STD), and skewness (SKEW)]. However, a discrepancy also shows that Mêdog has a smaller mean D_m (0.84 mm) than that of Nagqu (0.93 mm); additionally, Mêdog has a larger mean lgN_w (3.65) than that of Nagqu (3.58). When the raindrop diameter is larger than 1.0 mm, the occur-

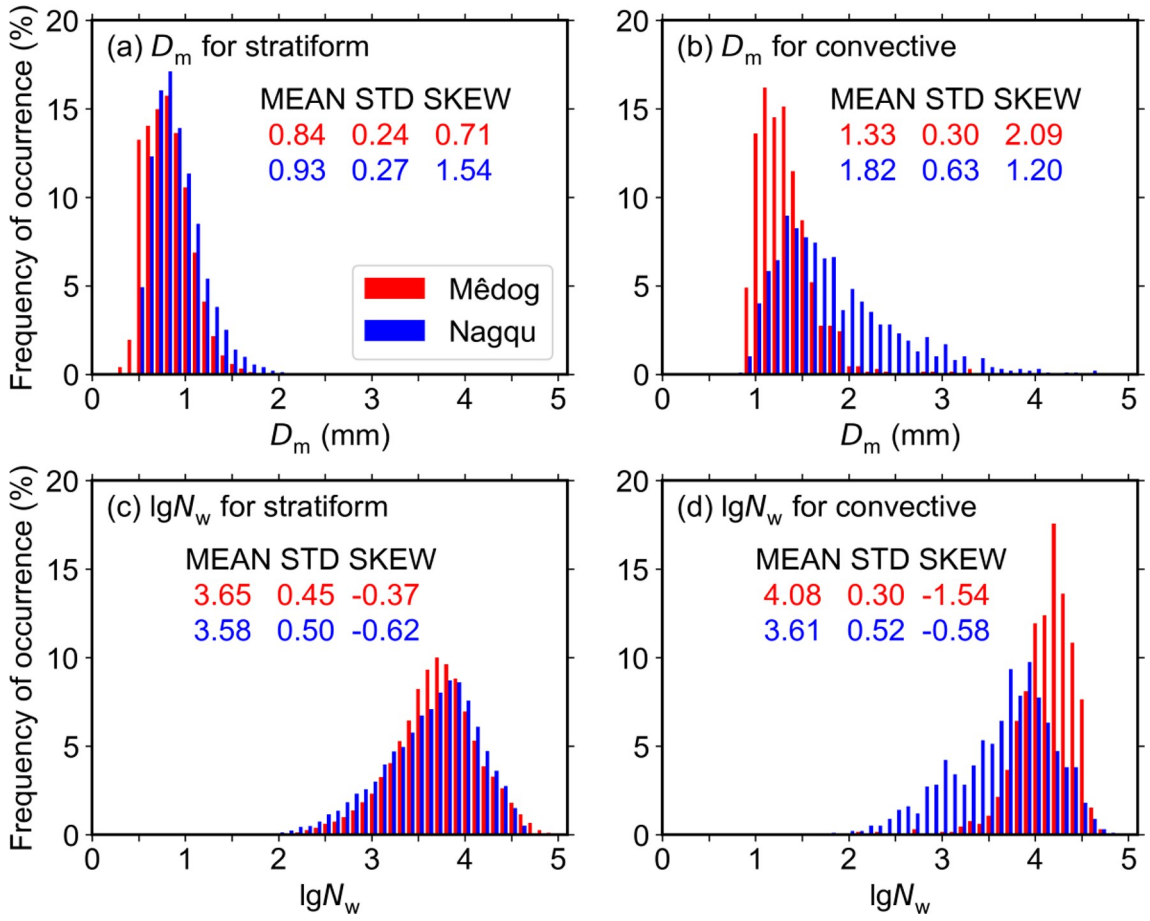

Fig. 7. Comparisons of occurrence frequencies between Mêdog (red) and Nagqu (blue): (a) D_m values for stratiform precipitation, (b) D_m values for convective precipitation, (c) lgN_w values for stratiform precipitation, and (d) lgN_w values for convective precipitation. The units of the D_m and N_w values are mm and mm^{-1} m^{-3}, respectively. Mean values (MEAN), standard deviations (STD), and skewness (SKEW) are given in the respective panels.

rence frequency of D_m in Nagqu is higher than that in Mêdog, suggesting larger raindrops in stratiform rain in Nagqu. This discrepancy may reflect microphysical differences in stratiform precipitation DSDs from Nagqu and Mêdog. Stratiform precipitation results from the melting of snowflakes and/or tiny, rimed ice particles. The low-density, large snow particles result in DSDs characterized by relatively larger D_m and lower N_w, compared to the tiny, rimed ice particles (Fabry and Zawadzki, 1995; Bringi et al., 2003).

On the other hand, the distributions of D_m and lgN_w for convective precipitation show significant differences between Mêdog and Nagqu (Figs. 7b and d). For instance, the D_m histogram representing convective precipitation in Nagqu is much broader than that of Mêdog, ranging from 1.0 mm to 3.5 mm with a mean value of 1.82 mm, which is similar to the range found for Colorado convective cases with a broader spectral width due to microphysical precipitation processes involving the melting of frozen particles (e.g., tiny hailstones and graupel) in the high plains (Bringi et al., 2003). In contrast, the Mêdog convective precipitation has a significantly narrower D_m distribution than that of Nagqu, ranging from 0.9 mm to 2.0 mm with a significantly smaller mean value of 1.33 mm, which is very close to the value of 1.41 mm measured in East China during the summer monsoon season (Wen et al., 2016). This similarity may be related to the warm and humid air currents in the two regions. The lgN_w histogram representing Nagqu is quite skewed, with a lower mean value of 3.61 (N_w ~ 4000 mm^{-1} m^{-3}), whereas the Mêdog histogram is nearly symmetric with a higher mean value of 4.08 (N_w ~ 12 000 mm^{-1} m^{-3}). On the whole, Mêdog convective rainfall is distinguished by relatively small mass-weighted mean diameter D_m but high normalized intercept parameter N_w, which is similar to the characteristics of tropical convective regimes due to sufficient water vapor supplies producing abundant small particles, whereas Nagqu had relatively larger D_m at lower N_w, reflecting the DSD characteristics of continental convective regimes.

Figures 7c and d show that the bimodality distribution of lgN_w is also obvious in Mêdog; this distribution has been found in tropical precipitation cases in previous studies (Ulbrich and Atlas, 2007; Thompson et al., 2015; Dolan et al., 2018). The occurrence frequency of lgN_w in Mêdog peaks at 3.6 and at 4.2, corresponding to stratiform and convective precipitation, respectively. This bimodal distribu-

tion is lacking in the convective and stratiform rainfall components in Nagqu.

To further understand the characteristics of the D_m and lgN_w values of stratiform and convective precipitation types in the two typical regions of the TP, we compared the results between Nagqu and Mêdog, as well as comparing the results with statistical results obtained for other climate regimes (Fig. 8). Two black rectangles in Fig. 8 correspond to the maritime- and continental-like convective clusters defined by Bringi et al. (2003), respectively. Stratiform (convective) precipitation cases are marked with blue (red) color symbols. The results indicate that the summer convective precipitation in Mêdog is maritime-like, exhibiting smaller D_m and higher lgN_w values, whereas the summer convective events in Nagqu could be identified as continental-like, characterized by relatively larger D_m and lower lgN_w values. Figure 8 also shows that the mean lgN_w values versus the mean D_m values for stratiform precipitation cases in Mêdog are close to those for Nagqu, which is in line with the report by Thompson et al. (2015) showing that stratiform rainfall in the tropics is similar to that in other climate regimes.

The results were also compared with other climate regimes in China (i.e., Nanjing in East China, Beijing in North China, and Foshan in South China, as reported by Wen et al., 2016, Ji et al., 2019, and Wang, 2019, respectively). For convective rain, Mêdog exhibited characteristics close to the two-dimensional video disdrometer observations of East and South China during the summer monsoon period, where the observed summer convective clusters are also maritime-like in nature. This may be due to the abundant warm and humid moisture in summer in the three regions, which produces large quantities of small particles. Nagqu consists of a lower concentration of relatively larger-sized drops, similar to that seen in North China, where the mean values of D_m and lgN_w are 2.03 mm and 3.61, respectively (Ji et al., 2019). The DSD characteristics in Nagqu and Beijing appear to be evidence of the microphysics of precipitation in the midlatitudes, where ice processes likely play an important role in precipitation processes (Dolan et al., 2018; Ji et al., 2019).

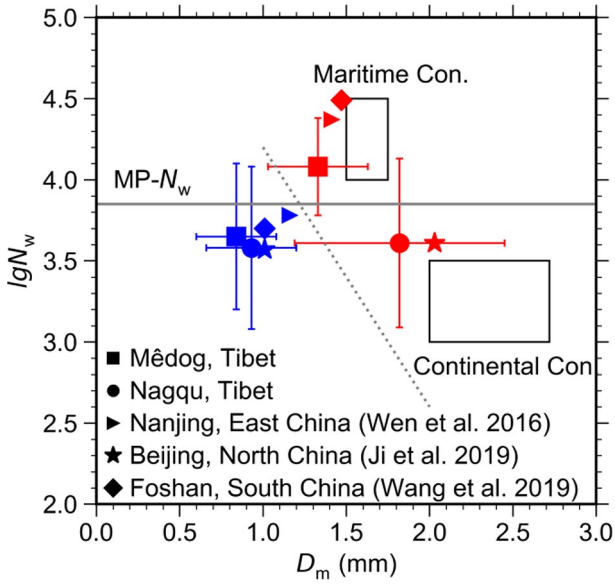

Fig. 8. Distribution of the mean values of lgN_w and D_m from the present study and from the literature, denoted with different symbols as shown in the legend. The blue/red symbols represent stratiform/convective precipitation. The two black rectangles represent the maritime and continental convective populations, respectively, from Bringi et al. (2003). The dotted and solid lines indicate the C–S separation lines from Bringi et al. (2003) for continental regions and from Thompson et al. (2015) for the tropics, respectively.

3.3. *The μ-Λ relation*

Previous studies have revealed that the μ-Λ relation has the ability to represent variability in DSDs of natural precipitation well, and can be approximately described by a second-degree polynomial (Zhang et al., 2003; Chen et al., 2017; Wu et al., 2019). The relation varies with climatological regimes, geographical locations, and precipitation types (Zhang et al., 2003; Cao et al., 2008; Chen et al., 2013, 2016).

Following the method of Zhang et al. (2003), to minimize the scatter, samples with drop counts > 1000 and rainfall rates $R > 5$ mm h^{-1} were used to compute the μ and Λ values in Mêdog and Nagqu. The μ-Λ relation can be used for the range of Λ between 0–20 mm^{-1}, and larger values of Λ indicate smaller raindrops (Zhang et al., 2003; Cao et al., 2008). Then, a second-degree polynomial μ-Λ relation was further fitted by the least squares method based on these data (Fig. 9). The relation for Mêdog is given below.

$$\Lambda = 0.0070\mu^2 + 0.932\mu + 1.528\,, \qquad (15)$$

The relation for Nagqu is as follows.

$$\Lambda = 0.0069\mu^2 + 0.881\mu + 1.733\,. \qquad (16)$$

Figure 9 shows that the shape factor μ of Mêdog is close to that of Nagqu when $\Lambda < 10$ mm^{-1}, while it is obviously lower than that of Nagqu when Λ is increasing. This could be related to higher numbers of small drops in Mêdog than in Nagqu.

Comparing the μ-Λ relations of Mêdog and Nagqu with that determined in Florida, USA, as derived by Zhang et al. (2003), the shape factor μ of Florida is distinctly smaller than those of Mêdog and Nagqu with increasing Λ (i.e., $\Lambda \geqslant 10$ mm^{-1}). On the one hand, these differences could be attributed partly to the different types of instruments used. The 1D PARSIVEL disdrometer used in our study tends to underestimate the numbers of small and midsize drops compared to the 2D video disdrometers used in the study in Florida, leading to larger μ values found in our study (Zhang et al., 2003; Wen et al., 2016). On the other hand, although a 1D PARSIVEL disdrometer was used in Mêdog and Nagqu, the μ-Λ relation obtained in Mêdog is slightly different from that determined in Nagqu, which implies that the microphysics of precipitation vary with geographical locations and climate regimes.

3.4. *QPE*

The major uncertainty in radar-based QPEs is caused by DSD variability, which can be affected by climate regimes, rainfall types, and geographical locations (Tokay and Short, 1996; Uijlenhoet, 2001; Rosenfeld and Ulbrich, 2003; Steiner et al., 2004; Lee and Zawadzki, 2005; Tokay et al., 2008). These DSD variabilities fundamentally affect the radar reflectivity factor (Z) and rainfall rate (R) relation, which is widely used in radar QPE algorithms. For example, Tokay and Short (1996) recommended the use of the relations $Z = 367R^{1.30}$ and $Z = 139R^{1.43}$ for stratiform and convective rainfall types in tropical regions, respectively. The Next-Generation Weather Radar (NEXRAD) system recommends the empirical relationships of $Z = 300R^{1.4}$ and $Z = 200R^{1.6}$ for convective and stratiform precipitation in the midlatitudes, respectively (Fulton et al., 1998). To improve radar rainfall estimates over the TP, the Z-R relations in Mêdog and Nagqu are discussed in this section based on the DSD characteristics observed during the rainy season.

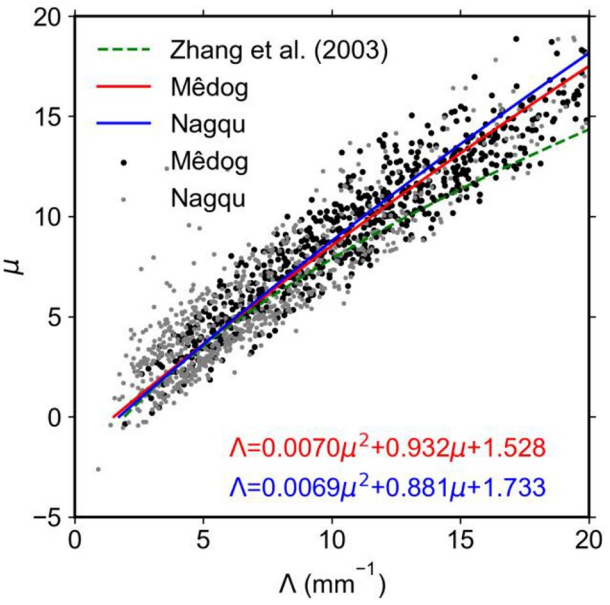

Fig. 9. Scatterplots of μ versus Λ and the empirical fitting relations for cases with rainfall rates >5 mm h^{-1} and raindrop counts > 1000 in Mêdog and Nagqu on the TP. The black dots represent Mêdog rainfall cases, and the gray dots represent Nagqu precipitation clusters. The red solid line and blue solid line indicate the fitted empirical μ-Λ relations in Mêdog and Nagqu, respectively. The green dashed line represents the empirical μ-Λ relation in Florida, obtained from Zhang et al. (2003).

Scatterplots displaying the relation between the Z and R are given in Fig. 10, superimposed with the Z-R fittings based on the least squares method for stratiform and convective precipitation cases in the two studied regions. Details of the fitted coefficients and exponents of the power-law relations for different precipitation types in the two regions are given in Table 1. For comparison with previous studies, the Z-R relations suggested in the midlatitudes and tropics are also superimposed upon Fig. 10 with differently colored solid lines. The corresponding power-law relationships are also given with the same colors as those of the solid lines. Following Wu et al., (2019), statistical parameters such as the normalized mean bias (NB) and normalized standard error (NSE) were used in this study to evaluate the performances of different Z-R relations.

The evaluation results are given in Table 2. In terms of stratiform rain, the fitted Z-R relation in Mêdog is close to that in Nagqu (Fig. 10a), which is fundamentally determ-

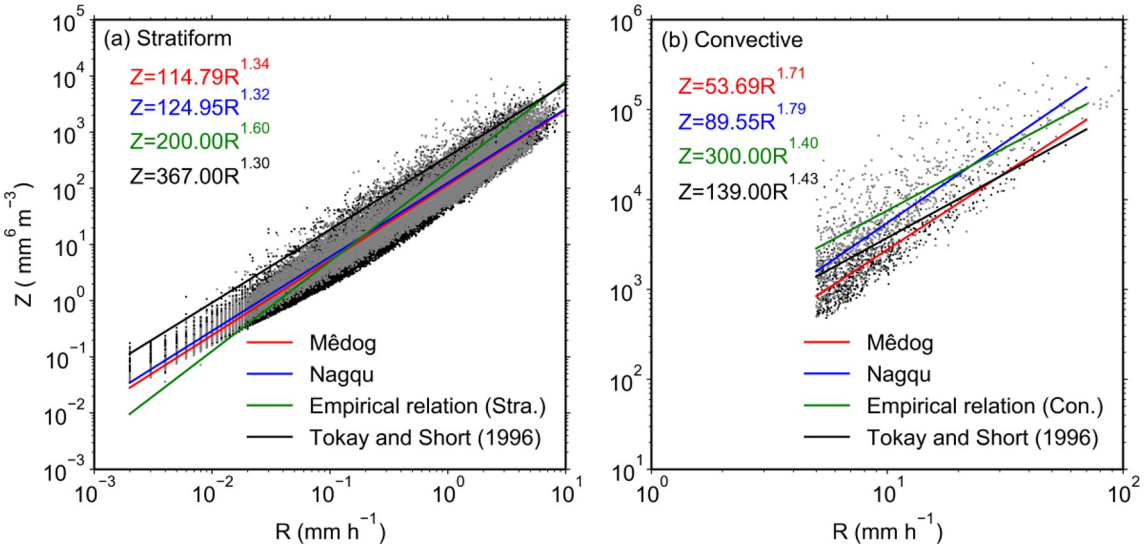

Fig. 10. Scatterplots of radar reflectivity (Z) versus rainfall rate (R), superimposed with the fitting curves for (a) stratiform rain and (b) convective rain. The black dots represent Mêdog rainfall cases, and the gray dots represent Nagqu precipitation clusters. The red and blue solid lines represent the fitting Z-R relations in Mêdog and Nagqu, respectively. The green solid lines denote the empirical relations used in NEXRAD. The black solid line represents the fitting relations from Tokay and Short (1996).

ined by the similar DSDs between the two regions (e.g., Figs. 7a, c, and 8). Table 2 shows that the minimum NB and NSE values in the two regions both come from the fitted *Z-R* relation, with NB values of 11.8% and 13.6% for Mêdog and Nagqu, respectively and NSE values of 24.8% and 28.3% for Mêdog and Nagqu, respectively. The empirical relationship at midlatitudes of $Z = 200R^{1.6}$ underestimated stratiform rain by 25.5% and 26.6% on average in Mêdog and Nagqu, respectively. In particular, stratiform precipitation was overestimated (underestimated) by approximately 16% and 22% (34% and 36%) in Mêdog and Nagqu, respectively, when the rain rate was below (above) 0.1 mm h^{-1}. Furthermore, the relation $Z = 367R^{1.30}$, suggested for use in the tropics (Tokay and Short, 1996), seriously underestimated stratiform precipitation, exceeding 50% in the two regions.

Comparing convective precipitation between the two regions, the fitted power-law relationships are $Z = 53.69R^{1.71}$ and $Z = 89.55R^{1.79}$ in Mêdog and Nagqu, respectively. Mêdog convective rain has smaller values for both the coefficient *A* and exponent *b*, likely associated with the relatively high concentration of small-sized raindrops in Mêdog. In other words, the same *Z* would derive a higher *R* in Mêdog, compared to Nagqu. In contrast with the *Z-R* empirical relations of $Z = 300R^{1.4}$ and $Z = 139R^{1.43}$, the fitted *Z-R* relation of Mêdog is close to $Z = 139R^{1.43}$, which was suggested for the tropics, and the *Z-R* relation of Nagqu approaches $Z = 300R^{1.4}$, which was recommended for the midlatitudes. The minimum NB and NSE values for convective rain in Mêdog and Nagqu are also obtained from the fitted *Z-R* relation, with NB values of 3.8% and 4.8% and NSE values of 20.6% and 31.3%, respectively. In addition, the use of the term $Z = 300R^{1.4}$ underestimates (overestimates) Nagqu convective precipitation by approximately 15% (20%) when the rainfall rate is below (above) 20 mm h^{-1}. The use of the term $Z = 139R^{1.43}$ also underestimates (overestimates) Mêdog convective precipitation by approximately 17% (5%) Mêdogwhen the rainfall rate is below (above) 30 mm h^{-1}.

Table 1. Fitted radar reflectivity and rain rate (*Z-R*) relations for stratiform and convective rain types in Mêdog and Nagqu on the Tibetan Plateau (TP).

	Stratiform rain		Convective rain	
Region	A	b	A	b
Mêdog	114.79	1.34	53.69	1.71
Nagqu	124.95	1.32	89.55	1.79

4. Discussion

The distinct discrepancies observed in the microphysical characteristics of precipitation between Mêdog and Nagqu could provide a good opportunity to evaluate and improve the parameterization schemes of models over the TP. Previous studies have shown that discrepancies in DSD characteristics are closely associated with the meteorological conditions of precipitation (Rao et al., 2009; Krishna et al, 2016; Wu et al., 2019; Zeng et al, 2019). To illustrate the possible mechanisms causing the observed variation in the microphysical characteristics of precipitation in Mêdog and Nagqu, some meteorological conditions are collected and analyzed. The mean values of the lifting condensation levels (LCLs), CTH, and 0°C isotherm levels during rainy days in Mêdog and Nagqu obtained from AWSs, MODIS products, and ECMWF ERA5 data are shown in Fig. 11. The mean relative humidity profiles for the rainy days obtained from ECMWF ERA5 data and the box and whisker plot of the surface wind speed are provided in Fig. 12.

The LCL can be approximately regarded as the cloud base height (CBH, Zeng et al., 2019). Following Lawrence (2005), LCLs were estimated from surface AWS data in this study. The 0°C isotherm levels were calculated from temperature profiles based on ERA5 reanalysis data. The average LCLs (CTHs) were 325 m (7500 m) and 833 m (6250 m) in Mêdog and Nagqu, respectively, while the mean 0°C isotherm levels were 4190 m and 1053 m, respectively.

The warm (cold) cloud depth is defined by the distance between the LCL (CTH) and 0°C isotherm level (Zeng et al., 2019). In Fig. 11, the LCL is lower in Mêdog than in Nagqu, and the 0°C isotherm level is much higher in Mêdog than in Nagqu. This reflects the microphysics of warm rain and the evolution of the DSD within a much deeper warm layer in Mêdog than in Nagqu. Previous studies have shown that the warm rain process differs from the cold rain process in the updraft, particle formation, and particle growth processes, resulting in different DSD characteristics (Rosenfeld and Ulbrich, 2003; Krishna et al., 2016; Zeng et al., 2019). Active coalescence is an important process in warm rain, contributing to high concentrations of size-limited raindrops (Dolan et al., 2018; Zeng et al., 2019). In general, in

Table 2. NB and NSE (%) values of empirical relations for convective/stratiform rain in the midlatitudes ($Z=300R^{1.40}/Z=200R^{1.60}$) and tropics ($Z=139R^{1.43}/Z=367R^{1.30}$) and of the fitted *Z-R* relation in this work for convective and stratiform precipitation types in Mêdog and Nagqu on the TP.

		Convective rain			Stratiform rain		
Parameter	Region	$Z=300R^{1.40}$	$Z=139R^{1.43}$	Fitted *Z-R*	$Z=200R^{1.60}$	$Z=367R^{1.30}$	Fitted *Z-R*
NB	Mêdog	−45.7	−10.9	3.8	−25.5	−53.7	11.8
	Nagqu	5.8	67.9	4.8	−26.6	−49.8	13.6
NSE	Mêdog	48.6	27.6	20.6	31.9	54.6	24.8
	Nagqu	40.3	77.1	31.3	36.0	52.8	28.3

Mêdog, warm cloud processes were prevalent, and the DSDs were characterized by large numbers of small raindrops during the rainy season, which could likely be related to the abundance of warm and moist air coming from the Indian Ocean during the summer monsoon period (Figs. 1, 5, 6, 7, and 8).

The cold rain process was dominant in Nagqu during the rainy season, as the LCL was close to the 0°C isotherm level, and the mean cold cloud depth was about 5000 m, in which ice particles grew rapidly. This may be attributed partly to the cold and dry air currents from the westerly winds and partly to water vapor loss during the transportation process from the Indian Ocean because of terrain elevation changes. Most raindrops in cold rain originate from melted ice particles such as graupel and/or hail, contributing to the formation of larger raindrops (Dolan et al., 2018; Zeng et al., 2019). Previous studies have also found that the microphysics of rain formation in the high plains involve the melting of graupel and tiny hailstones (Bringi et al., 2003; Fu et al., 2007; Li et al., 2014). As shown in Figs. 5 and 6, the increased rainfall rate in Nagqu may be mainly attributed to an increase in raindrop size.

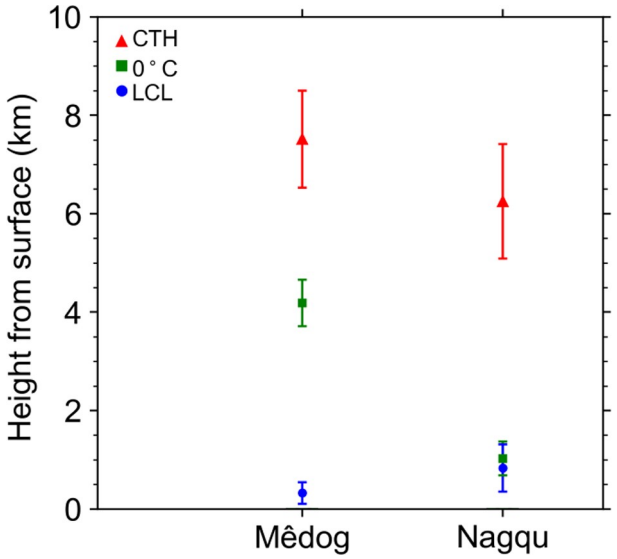

Fig. 11. Mean heights of the CTH, 0°C isotherm, and LCL. The red triangles are the mean CTH values, the green rectangles represent the average heights of 0°C isotherm levels, and the blue circles indicate mean LCL values. The error bars represent ±3 times the standard deviation.

In addition, Nagqu also experienced lower humidity (Fig. 12a) and higher wind speeds near the land surface than did Mêdog (Fig. 12b). Humidity and wind are two primary meteorological factors that affect evaporation (McVicar et al., 2012; Wu et al., 2019). It is evident that evaporation processes are stronger in Nagqu than in Mêdog. The evaporation process would contribute to a lower number of small drops when atmospheric conditions are relatively dry (Atlas and Ulbrich, 2000). Instead, the evaporation in Mêdog is weak, which is associated with larger humidity values and weaker wind speeds and leads to the production of many small drops.

5. Summary and conclusions

The geographical locations, water vapor sources, and climatic characteristics of Mêdog and Nagqu are quite different, and these factors fundamentally determine the distinct DSD characteristics in the two regions of the TP. DSD measurements were obtained in Nagqu and Mêdog using a PASIVEL disdrometer during the third TIPEX and STEPS projects and, along with ECMWF EAR5 reanalysis data, MODIS products, and AWS data, used to understand the observed microphysical characteristics of two typical regions of the TP. The findings can be summarized as fol-

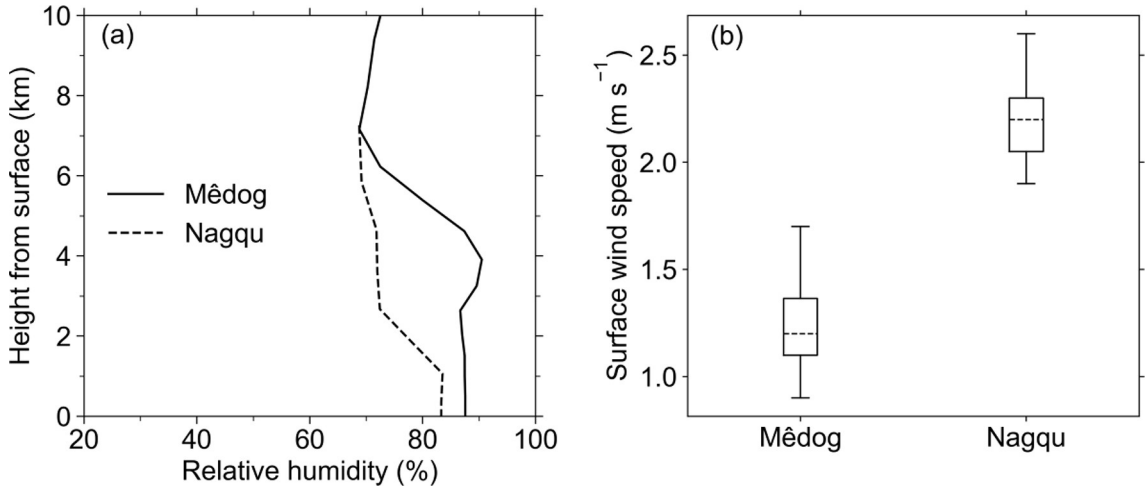

Fig. 12. (a) Diagrams of the mean profiles of relative humidity (%) for rainy days in Mêdog (solid lines) and Nagqu (dashed lines) on the TP obtained from ECMWF EAR5 reanalysis data during the observation period used in this study; (b) Box and whisker plot of surface wind speeds obtained from automated weather stations. The centerline of each box, shown in dashed lines, represents the median, and the bottom and top lines of each box indicate the 25th and 75th percentiles, respectively.

lows.

(1) The number concentrations of small raindrops are higher in Mêdog than in Nagqu, whereas Nagqu has higher concentrations of large raindrops than does Mêdog. A significant difference in the DSDs between Mêdog and Nagqu shows that large rainfall rate categories (i.e., $R > 5$ mm h^{-1}) present two peak distributions in Mêdog; this feature is lacking in Nagqu. The fitted gamma parameters showed that Nagqu has larger (lower) D_m (lgN_w) values than Mêdog does for all rainfall rate categories. Furthermore, the difference in D_m values between the Nagqu and Mêdog regions increases with an increasing rainfall rate.

(2) The DSD characteristics of different rain types show that stratiform precipitation has a similar distribution in the two studied regions, whereas the convective precipitation distribution is significantly different between the two regions of the TP. The mean D_m (lgN_w) value is higher (lower) for convective precipitation in Nagqu than in Mêdog. Overall, convective precipitation in Nagqu can be identified as continental-like, characterized by a relatively larger mean D_m value of 1.82 mm and lower mean lgN_w value of 3.61 compared to those in Mêdog, while convective precipitation in Mêdog can be identified as maritime-like, characterized by a relatively smaller mean D_m value of 1.33 mm and a higher mean lgN_w value of 4.08. The characteristic bimodality of the lgN_w distribution was observed in Mêdog, corresponding to convective and stratiform precipitation cases. This bimodality was lacking in Nagqu.

(3) A fitted second-degree polynomial μ-Λ relation was also derived. With increasing Λ (e.g., $\Lambda > 10$ mm^{-1}), the shape parameter μ of Mêdog is distinctly smaller than that of Nagqu if the same Λ is given, which is probably related to the higher concentration of small raindrops in Mêdog. DSD variability fundamentally determines the diversity of the Z-R relation. The Z-R relation for stratiform precipitation in Mêdog is close to that in Nagqu, while that for convective precipitation is significantly different in Mêdog than that in Nagqu. This feature is consistent with the DSD characteristics of stratiform and convective precipitation observed in Mêdog and Nagqu. For convective precipitation, Mêdog has both a smaller coefficient A and exponent b of the Z-R relation compared to Nagqu, indicating a higher rainfall efficiency in Mêdog than in Nagqu for the same radar reflectivity.

(4) The discrepancy in the DSDs of Mêdog and Nagqu is closely associated with the meteorological conditions of the two regions. The warm rain process is prevalent in Mêdog, producing high concentrations of small-size raindrops via active coalescence, whereas cold rain microphysics are dominant in Nagqu, contributing to lower concentrations of large raindrops formed by the melting of ice particles. In addition, the lower humidity and larger surface wind speed values in Nagqu compared to those in Mêdog tend to induce evaporation processes, leading to fewer small drops.

In general, Mêdog is dominated by maritime-like convective precipitation and warm rain processes in summer, which could be mainly attributed to the warm and humid airflow brought by the Indian Ocean monsoon. Continental-like convective precipitation and cold rain processes prevail in summer in Nagqu, partly due to the cold and dry air brought to the area by westerly winds and partly due to the water vapor loss during the transportation process from the Indian Ocean because of an increase in terrain altitude.

Notably, the results of this work are based on disdrometer data. Because a K-band Micro Rain Radar was deployed in Mêdog in July 2019, the vertical characteristics of DSDs will be investigated in future research by joint measurements. Additionally, DSD characteristics observed during different seasons should be considered for comparative research.

Acknowledgements. This work was supported by the Second Tibetan Plateau Scientific Expedition and Research (STEP) program (Grant No. 2019QZKK0105) and the National Natural Science Foundation of China (Grant No. 41775036).

REFERENCES

Atlas, D., and C. W. Ulbrich, 2000: An observationally based conceptual model of warm oceanic convective rain in the tropics. *J. Appl. Meteorol.*, **39**, 2165–2181, https://doi.org/10.1175/1520-0450(2001)040<2165:AOBCMO>2.0.CO;2.

Atlas, D., R. C. Srivastava, and R. S. Sekhon, 1973: Doppler radar characteristics of precipitation at vertical incidence. *Rev. Geophys.*, **11**, 1–35, https://doi.org/10.1029/RG011i001p00001.

Bringi, V. N., V. Chandrasekar, J. Hubbert, E. Gorgucci, W. L. Randeu, and M. Schoenhuber, 2003: Raindrop size distribution in different climatic regimes from disdrometer and dual-polarized radar analysis. *J. Atmos. Sci.*, **60**, 354–365, https://doi.org/10.1175/1520-0469(2003)060<0354:RSDIDC>2.0.CO;2.

Cao, Q., G. F. Zhang, E. Brandes, T. Schuur, A. Ryzhkov, and K. Ikeda, 2008: Analysis of video disdrometer and polarimetric radar data to characterize rain microphysics in Oklahoma. *J. Appl. Meteor. Climatol.*, **47**(8), 2238–2255, https://doi.org/10.1175/2008JAMC1732.1.

Chandrasekar, V., W. Y. Li, and B. Zafar, 2005: Estimation of raindrop size distribution from spaceborne radar observations. *IEEE Trans. Geosci. Remote Sens.*, **43**(5), 1078–1086, https://doi.org/10.1109/TGRS.2005.846130.

Chang, Y., and X. L. Guo, 2016: Characteristics of convective cloud and precipitation during summer time at Naqu over Tibetan Plateau. *Chinese Science Bulletin*, **61**(15), 1706–1720, https://doi.org/10.1360/N972015-01292.

Chen, B. J., J. Yang, and J. P. Pu, 2013: Statistical characteristics of raindrop size distribution in the Meiyu season observed in eastern China. *J. Meteor. Soc. Japan*, **91**(2), 215–227, https://doi.org/10.2151/jmsj.2013-208.

Chen, B. J., J. Wang, and D. L. Gong, 2016: Raindrop size distribution in a midlatitude continental squall line measured by Thies optical disdrometers over East China. *J. Appl. Meteor. Climatol.*, **55**, 621–634, https://doi.org/10.1175/JAMC-D-15-0127.1.

Chen, B. J., Z. Q. Hu, L. P. Liu, and G. F. Zhang, 2017: Rain-

drop size distribution measurements at 4,500 m on the Tibetan Plateau during TIPEX-III. *J. Geophys. Res.*, **122**, 11 092–11 106, https://doi.org/10.1002/2017JD027233.

Chen, P., and B. Li, 2018: Characteristics of water vapor transport and its influence in Southeast Tibet. *South China Agriculture*, **12**, 124–125, https://doi.org/10.19415/j.cnki.1673-890x.2018.09.066. (in Chinese)

Cifelli, R., V. Chandrasekar, S. Lim, P. C. Kennedy, Y. Wang, and S. A. Rutledge, 2011: A new dual-polarization radar rainfall algorithm: Application in Colorado precipitation events. *J. Atmos. Ocean. Technol.*, **28**, 352–364, https://doi.org/10.1175/2010JTECHA1488.1.

Dolan, B., B. Fuchs, S. A. Rutledge, E. A. Barnes, and E. J. Thompson, 2018: Primary modes of global drop size distributions. *J. Atmos. Sci.*, **75**, 1453–1476, https://doi.org/10.1175/JAS-D-17-0242.1.

Fabry, F., I. Zawadzki, 1995: Long-term radar observations of the melting layer of precipitation and their interpretation. *J. Atmos. Sci.*, **52**, 838–851, https://doi.org/10.1175/1520-0469(1995)052<0838:LTROOT>2.0.CO;2.

Friedrich, K., S. Higgins, F. J. Masters, and C. R. Lopez, 2013: Articulating and stationary PARSIVEL disdrometer measurements in conditions with strong winds and heavy rainfall. *J. Atmos. Ocean. Technol.*, **30**, 2063–2080, https://doi.org/10.1175/JTECH-D-12-00254.1.

Fu, Y. F., H. T. Li, and Y. Zi, 2007: Case study of precipitation cloud structure viewed by TRMM satellite in a valley of the Tibetan Plateau. *Plateau Meteorology*, **26**, 98–106, https://doi.org/10.3321/j.issn:1000-0534.2007.01.012. (in Chinese with English abstract)

Fulton, R. A., J. P. Breidenbach, D. J. Seo, D. A. Miller, and T. O'Bannon, 1998: The WSR-88D rainfall algorithm. *Wea. Forecasting*, **13**, 377–395, https://doi.org/10.1175/1520-0434(1998)013<0377:TWRA>2.0.CO;2.

Gilmore, M. S., J. M. Straka, and E. N. Rasmussen, 2004: Precipitation uncertainty due to variations in precipitation particle parameters within a simple microphysics scheme. *Mon. Wea. Rev.*, **132**, 2610–2627, https://doi.org/10.1175/MWR2810.1.

Gossard, E. E., R. O. Strauch, and R. R. Rogers, 1990: Evolution of dropsize distributions in liquid precipitation observed by ground-based Doppler radar. *J. Atmos. Ocean. Technol.*, **7**, 815–828, https://doi.org/10.1175/1520-0426(1990)007<0815:EODDIL>2.0.CO;2.

Huo, Z. Y., Z. Ruan, M. Wei, R. S. Ge, F. Li, and Y. Ruan, 2019: Statistical characteristics of raindrop size distribution in South China summer based on the vertical structure derived from VPR-CFMCW. *Atmospheric Research*, **222**, 47–61, https://doi.org/10.1016/j.atmosres.2019.01.022.

Jaffrain, J., and A. Berne, 2011: Experimental quantification of the sampling uncertainty associated with measurements from PARSIVEL disdrometers. *J. Hydrometeor.*, **12**, 352–370, https://doi.org/10.1175/2010JHM1244.1.

Ji, L., H. N. Chen, L. Li, B. J. Chen, X. Xiao, M. Chen, and G. F. Zhang, 2019: Raindrop size distributions and rain characteristics observed by a PARSIVEL disdrometer in Beijing, northern China. *Remote Sensing*, **11**, 1479, https://doi.org/10.3390/rs11121479.

Kang, S. C., Y. W. Xu, Q. L. You, W. A. Flügel, N. Pepin, and T. D. Yao, 2010: Review of climate and cryospheric change in the Tibetan Plateau. *Environmental Research Letters*, **5**(1), 015101, https://doi.org/10.1088/1748-9326/5/1/015101.

Kozu, T., and K. Nakamura, 1991: Rainfall parameter estimation from dual-radar measurements combining reflectivity profile and path-integrated attenuation. *J. Atmos. Ocean. Technol.*, **8**, 259–271, https://doi.org/10.1175/1520-0426(1991)008<0259:RPEFDR>2.0.CO;2.

Krajewski, W. F., and Coauthors, 2006: DEVEX-disdrometer evaluation experiment: Basic results and implications for hydrologic studies. *Advances in Water Resources*, **29**, 311–325, https://doi.org/10.1016/j.advwatres.2005.03.018.

Krishna, U. V. M., K. K. Reddy, B. K. Seela, R. Shirooka, and P. L. Lin, 2016: Raindrop size distribution of easterly and westerly monsoon precipitation observed over Palau islands in the Western Pacific Ocean. *Atmospheric Research*, **174–175**, 41–51, https://doi.org/10.1016/j.atmosres.2016.01.013.

Lam, H. Y., J. Din, and S. L. Jong, 2015: Statistical and physical descriptions of raindrop size distributions in equatorial Malaysia from disdrometer observations. *Advances in Meteorology*, **2015**, 253730, https://doi.org/10.1155/2015/253730.

Lawrence, M. G., 2005: The relationship between relative humidity and the dewpoint temperature in moist air: A simple conversion and applications. *Bull. Am. Meteor. Soc.*, **86**, 225–233, https://doi.org/10.1175/BAMS-86-2-225.

Lee, C. K., and I. Zawadzki, 2005: Variability of drop size distributions: Time - scale dependence of the variability and its effects on rain estimation. *J. Appl. Meteor.*, **44**, 241–255, https://doi.org/10.1175/JAM2183.1.

Li, D., A. J. Bai, Y. J. Xue, et al., 2014: Comparative analysis on characteristics of summer convective precipitation over Tibetan Plateau and Sichuan Basin. *Meteorological Monthly*, **40**, 280–289, https://doi.org/10.7519/j.issn.1000-0526.2014.03.003. (in Chinese with English abstract)

Li, J., 2018: Hourly station-based precipitation characteristics over the Tibetan Plateau. *International Journal of Climatology*, **38**, 1560–1570, https://doi.org/10.1002/joc.5281.

List, R., N. R. Donaldson, and R. E. Stewart, 1987: Temporal evolution of drop spectra to collisional equilibrium in steady and pulsating rain. *J. Atmos. Sci.*, **44**, 362–372, https://doi.org/10.1175/1520-0469(1987)044<0362:TEODST>2.0.CO;2.

Liu, L. P., J. M. Feng, R. Z. Chu, Y. J. Zhou, and K. Ueno, 2002: The diurnal variation of precipitation in monsoon season in the Tibetan Plateau. *Adv. Atmos. Sci.*, **19**(2), 365–378, https://doi.org/10.1007/s00376-002-0028-6.

Liu, L. P., J. F. Zheng, Z. Ruan, Z. H. Cui, Z. Q. Hu, S. H. Wu, G. Y. Dai, and Y. H. Wu, 2015: The preliminary analyses of the cloud properties over the Tibetan Plateau from the field experiments in clouds precipitation with the vavious radars. *Acta Meteorologica Sinica*, **74**(4), 635–647, https://doi.org/10.11676/qxxb2015.041. (in Chinese with English abstract)

Maki, M., T. D. Keenan, Y. Sasaki, and K. Nakamura, 2001: Characteristics of the raindrop size distribution in tropical continental squall lines observed in Darwin, Australia. *J. Appl. Meteor.*, **40**(8), 1393–1412, https://doi.org/10.1175/1520-0450(2001)040<1393:COTRSD>2.0.CO;2.

McVicar, T. R., and Coauthors, 2012: Global review and synthesis of trends in observed terrestrial near-surface wind speeds: Implications for evaporation. *J. Hydrol*, **416–417**, 182–205, https://doi.org/10.1016/j.jhydrol.2011.10.024.

Milbrandt, J. A., and M. K. Yau, 2005: A multimoment bulk microphysics parameterization. *Part I: Analysis of the role of the spectral shape parameter. J. Atmos. Sci.*, **62**, 3051–3064, https://doi.org/10.1175/JAS3534.1.

Morrison, H., and J. A. Milbrandt, 2015: Parameterization of

cloud microphysics based on the prediction of bulk ice particle properties. Part I: Scheme description and idealized tests. *J. Atmos. Sci.*, **72**, 287–311, https://doi.org/10.1175/JAS-D-14-0065.1.

Niu, S. J., X. C. Jia, J. R. Sang, X. L. Liu, C. S. Lu, and Y. G. Liu, 2010: Distributions of raindrop sizes and fall velocities in a semiarid plateau climate: Convective versus stratiform rains. *J. Appl. Meteor. Climatol.*, **49**, 632–645, https://doi.org/10.1175/2009JAMC2208.1.

Porcù, F., L. P. D'Adderio, F. Prodi, and C. Caracciolo, 2014: Rain drop size distribution over the Tibetan Plateau. *Atmospheric Research*, **150**, 21–30, https://doi.org/10.1016/j.atmosres.2014.07.005.

Rao, T. N., B. Radhakrishna, K. Nakamura, and N. P. Rao, 2009: Differences in raindrop size distribution from southwest monsoon to northeast monsoon at Gadanki. *Quart. J. Roy. Meteor. Soc.*, **135**, 1630–1637, https://doi.org/10.1002/qj.432.

Rosenfeld, D., and C. W. Ulbrich, 2003: Cloud microphysical properties, processes, and rainfall estimation opportunities. *Radar and Atmospheric Science: A Collection of Essays in Honor of David Atlas*, R. M. Wakimoto and R. Srivastava, Eds., Springer, 237–258, https://doi.org/10.1007/978-1-878220-36-3_10.

Smith, P. L., 2003: Raindrop size distributions: Exponential or gamma-does the difference matter. *J. Appl. Meteor.*, **42**, 1031–1034, https://doi.org/10.1175/1520-0450(2003)042<1031:RSDEOG>2.0.CO;2.

Srivastava, R. C., 1971: Size distribution of raindrops generated by their breakup and coalescence. *J. Atmos. Sci.*, **28**, 410–415, https://doi.org/10.1175/1520-0469(1971)028<0410:SDORGB>2.0.CO;2.

Steiner, M., and A. Waldvogel, 1987: Peaks in Raindrop size distributions. *J. Atmos. Sci.*, **44**, 3127–3133, https://doi.org/10.1175/1520-0469(1987)044<3127:PIRSD>2.0.CO;2.

Steiner, M., J. A. Smith, and R. Uijlenhoet, 2004: A microphysical interpretation of radar reflectivity–rain rate relationships. *J. Atmos. Sci.*, **61**, 1114–1131, https://doi.org/10.1175/1520-0469(2004)061<1114:AMIORR>2.0.CO;2.

Tang, Q., H. Xiao, C. W. Guo, and L. Feng, 2014: Characteristics of the raindrop size distributions and their retrieved polarimetric radar parameters in northern and southern China. *Atmospheric Research*, **135–136**, 59–75, https://doi.org/10.1016/j.atmosres.2013.08.003.

Testud, J., S. Oury, R. A. Black, P. Amayenc, and X. K. Dou, 2001: The concept of "normalized" distribution to describe raindrop spectra: A tool for cloud physics and cloud remote sensing. *J. Appl. Meteor.*, **40**(6), 1118–1140, https://doi.org/10.1175/1520-0450(2001)040<1118:TCONDT>2.0.CO;2.

Thompson, E. J., S. A. Rutledge, B. Dolan, and M. Thurai, 2015: Drop size distributions and radar observations of convective and stratiform rain over the equatorial Indian and west Pacific Oceans. *J. Atmos. Sci.*, **72**, 4091–4125, https://doi.org/10.1175/JAS-D-14-0206.1.

Thurai, M., V. N. Bringi, and P. T. May, 2010: CPOL radar-derived drop size distribution statistics of stratiform and convective rain for two regimes in Darwin, Australia. *J. Atmos. Ocean. Technol.*, **27**, 932–942, https://doi.org/10.1175/2010JTECHA1349.1.

Tokay, A., and D. A. Short, 1996: Evidence from tropical raindrop spectra of the origin of rain from stratiform versus convective clouds. *J. Appl. Meteor.*, **35**, 355–371, https://doi.org/10.1175/1520-0450(1996)035<0355:EFTRSO>2.0.CO;2.

Tokay, A., P. G. Bashor, E. Habib, and T. Kasparis, 2008: Raindrop size distribution measurements in tropical cyclones. *Mon. Wea. Rev.*, **136**(5), 1669–1685, https://doi.org/10.1175/2007MWR2122.1.

Tokay, A., W. A. Petersen, P. Gatlin, and M. Wingo, 2013: Comparison of raindrop size distribution measurements by collocated disdrometers. *J. Atmos. Ocean. Technol.*, **30**, 1672–1690, https://doi.org/10.1175/JTECH-D-12-00163.1.

Uijlenhoet, R., 2001: Raindrop size distributions and radar reflectivity-rain rate relationships for radar hydrology. *Hydrology and Earth System Sciences*, **5**, 615–627, https://doi.org/10.5194/hess-5-615-2001.

Ulbrich, C. W., 1983: Natural variations in the analytical form of the raindrop size distribution. *J. Climate Appl. Meteor.*, **22**, 1764–1775, https://doi.org/10.1175/1520-0450(1983)022<1764:NVITAF>2.0.CO;2.

Ulbrich, C. W., and D. Atlas, 2007: Microphysics of raindrop size spectra: Tropical continental and maritime storms. *J. Appl. Meteor. Climatol.*, **46**, 1777–1791, https://doi.org/10.1175/2007JAMC1649.1.

Wan, B. C., Z. Q. Gao, F. Chen, and C. G. Lu, 2017: Impact of Tibetan Plateau surface heating on persistent extreme precipitation events in southeastern China. *Mon. Wea. Rev.*, **145**(9), 3485–3505, https://doi.org/10.1175/MWR-D-17-0061.1.

Wang, D. H., J. F. Yin, and G. Q. Zhai, 2015: In-situ measurements of cloud - precipitation microphysics in the East Asian monsoon region since 1960. *J. Meteor. Res.*, **29**, 155–179, https://doi.org/10.1007/s13351-015-3235-7.

Wang, M. Y., 2019: Effects of synoptic weather patterns and pollution on microphysical characteristics of precipitation in East and South China during warm season. M.S. thesis, Nanjing University.

Wen, L., K. Zhao, G. F. Zhang, M. Xue, B. W. Zhou, S. Liu, and X. C. Chen, 2016: Statistical characteristics of raindrop size distributions observed in East China during the Asian summer monsoon season using 2-D video disdrometer and Micro Rain Radar data. *J. Geophys. Res.*, **121**, 2265–2282, https://doi.org/10.1002/2015JD024160.

Wen, L., K. Zhao, G. F. Zhang, S. Liu, and G. Chen, 2017: Impacts of instrument limitations on estimated raindrop size distribution, radar parameters, and model microphysics during Mei-Yu season in East China. *J. Atmos. Ocean. Technol.*, **34**, 1021–1037, https://doi.org/10.1175/JTECH-D-16-0225.1.

Wu, Y. H., and L. P. Liu, 2017: Statistical characteristics of raindrop size distribution in the Tibetan Plateau and southern China. *Adv. Atmos. Sci.*, **34**, 727–736, https://doi.org/10.1007/s00376-016-5235-7.

Wu, Z. H., Y. Zhang, L. F. Zhang, H. C. Lei, Y. Q. Xie, L. Wen, and J. F. Yang, 2019: Characteristics of summer season raindrop size distribution in three typical regions of western Pacific. *J. Geophys. Res.*, **124**, 4054–4073, https://doi.org/10.1029/2018JD029194.

Xu, X. D., C. G. Lu, X. H. Shi, and S. T. Gao, 2008: World water tower: An atmospheric perspective. *Geophys. Res. Lett.*, **35**(20), L20815, https://doi.org/10.1029/2008GL035867.

Xu, X. D., T. L. Zhao, C. G. Lu, and X. H. Shi, 2014: Characteristics of the water cycle in the atmosphere over the Tibetan Plateau. *Acta Meteorologica Sinica*, **72**(6), 1079–1095, https://doi.org/10.11676/qxxb2014.091. (in Chinese with English abstract)

Xu, X. D., T. L. Zhao, X. H. Shi, and C. G. Lu, 2015: A study of the role of the Tibetan Plateau's thermal forcing in modulating rainband and moisture transport in eastern China. *Acta Meteorologica Sinica*, **73**(1), 20–35, https://doi.org/10.11676/qxxb2014.051. (in Chinese with English abstract)

Yang, Y. C., D. Y. Gao, and B. S. Li, 1987: Preliminary study of water vapor pass along the downstream of Yarlung Zangbo. *Scientia Sinica B*, **17**(8), 893–902, https://doi.org/10.1360/zb1987-17-8-893. (in Chinese)

Yuter, S. E., and R. A. Houze Jr., 1997: Measurements of raindrop size distributions over the Pacific warm pool and implications for *Z–R* relations. *J. Appl. Meteor.*, **36**(7), 847–867, https://doi.org/10.1175/1520-0450(1997)036<0847:MORSDO>2.0.CO;2.

Yuter, S. E., D. E. Kingsmill, L. B. Nance, and M. Löffler-Mang, 2006: Observations of precipitation size and fall speed characteristics within coexisting rain and wet snow. *J. Appl. Meteor. Climatol.*, **45**, 1450–1464, https://doi.org/10.1175/JAM2406.1.

Zeng, Q. W., Y. Zhang, H. C. Lei, Y. Q. Xie, T. C. Gao, L. F. Zhang, C. M. Wang, and Y. B. Huang, 2019: Microphysical characteristics of precipitation during pre-monsoon, monsoon, and post-monsoon periods over the South China Sea. *Adv. Atmos. Sci.*, **36**(10), 1103–1120, https://doi.org/10.1007/s00376-019-8225-8.

Zeng, Y. T., Y. Zhang, K. Zhou, Y. Q. Yao, and L. F. Yang, 2020: Analysis on the source and transport characteristics of moisture in Naqu of the Qinghai-Tibetan Plateau in summer. *Plateau Meteorology*, **39**(3), 467–476, https://doi.org/10.7522/j.issn.1000-0534.2019.00120. (in Chinese with English abstract)

Zhang, G., J. Vivekanandan, and E. Brandes, 2001: A method for estimating rain rate and drop size distribution from polarimetric radar measurements. *IEEE Trans. Geosci. Remote Sens.*, **39**(4), 830–841, https://doi.org/10.1109/36.917906.

Zhang, G. F., J. Vivekanandan, E. A. Brandes, R. Meneghini, and T. Kozu, 2003: The shape–slope relation in observed gamma raindrop size distributions: Statistical error or useful information. *J. Atmos. Ocean. Technol.*, **20**, 1106–1119, https://doi.org/10.1175/1520-0426(2003)020<1106:TSRIOG>2.0.CO;2.

Zhang, W. X., L. X. Zhang, and T. J. Zhou, 2016: Interannual variability and the underlying mechanism of summer precipitation over the Yarlung Zangbo River basin. *Chinese Journal of Atmospheric Sciences*, **40**(5), 965–980, https://doi.org/10.3878/j.issn.1006-9895.1512.15205. (in Chinese with English abstract)

Zhao, P., and Coauthors, 2018: The Tibetan Plateau surface-atmosphere coupling system and its weather and climate effects: The Third Tibetan Plateau Atmospheric Scientific Experiment. *Acta Meteorologica Sinica*, **76**(6), 833–860, https://doi.org/10.11676/qxxb2018.060. (in Chinese with English abstract)

Zhao, P., and Coauthors, 2019: The Tibetan Plateau surface- atmosphere coupling system and its weather and climate effects: The Third Tibetan Plateau atmospheric science experiment. *J. Meteor. Res.*, **33**, 375–399, https://doi.org/10.1007/s13351-019-8602-3.